

SARTA CLOUDY: A Fast Forward Model Version of SARTA with Cloud/Aerosol Scattering

S. De Souza-Machado, L. L. Strow, S. E. Hannon
University of Maryland Baltimore County, Baltimore, MD 21250 USA

March 1, 2013

Abstract

The SARTA CLOUDY code is a modification of the UMBC clear sky SARTA code, allowing users to compute synthetic infrared radiances for the AIRS instrument, in the presence of clouds and aerosols. By re-parameterizing the cloud scattering parameters into effective optical depths, the effect of clouds on upwelling radiation from the Earth's atmosphere is effectively recast as that of (an) additional absorbing gas(es), which allows us to use the efficient radiative transfer algorithm of the clear sky code. The liens of the code are that model vertical cloud fields (from eg ECMWF) need to be reshaped into at most two slab clouds. However, comparisons against packages which uses sophisticated algorithms (eg maximal overlap clouds and scattering trained on DISORT algorithm) shows that the SARTA CLOUDY code produces radiances accurate to about 3K (converted to equivalent Brightness Temperature)

1 Introduction

This document gives an overview of SARTA-CLOUDY, which is a Fast Infrared Atmospheric Radiative Transfer algorithm, written to simply but accurately account for the effects of scattering by aerosols and clouds. This scattering package is directly based on our clear sky fast algorithm SARTA, and so should be relatively straightforward for users familiar with the clear sky version, to integrate and use. In addition, the code is based on treating the effects of cloud and aerosols as that of additional absorptive gases, which means the radiative transfer retains its speed and efficiency.

We begin by outlining the clear sky monochromatic algorithm, followed by a discussion of the scattering model we chose to use for the monochromatic case. We then follow with a brief discussion of the challenges in making a code for polychromatic clear sky transfer, and how the scattering algorithm can be easily adapted to work in this polychromatic case as well.

We have already successfully used the scattering code to retrieve dust loadings and heights, for individual AIRS Fields-of-Views [1]. Assuming we knew the height of the dust layer, using a handful of AIRS channels, three iterations for convergence were done in a matter of milliseconds, for each AIRS pixel. We envision a similar approach for an operational retrieval, which we discuss. A discussion of how we implement Numerical Weather Prediction model fields for use in our algorithm then follows.

We then show comparisons of window channel radiances computed using ECMWF/ERA fields, versus actual AIRS observations. Finally we show comparisons of radiances produced by SARTA-CLOUDY versus those produced by a more sophisticated algorithm, and argue that

for operational retrieval of temperature and humidity, the accuracy of our code is more than sufficient.

2 Monochromatic Clear sky Radiative transfer algorithm

As a monochromatic beam of radiation propagates through a layer, the change in diffuse beam intensity $R_{\mu} \dots$ in a plane parallel medium is given by the standard Schwarzschild equation [1, 2, 3]

$$\frac{dR_{\mu} \dots}{dk_e} = f_{\mu} R_{\mu} \dots + J_{\mu} \dots \quad (1)$$

where μ is the cosine of the viewing angle, k_e is the extinction optical depth, k is the wavenumber and $J_{\mu} \dots$ is the source function. For a nonscattering "clear sky", the source function is usually the Planck emission $B_{\mu}; T \dots$ at the layer temperature T , leading to an equation that can easily be solved for an individual layer. Dividing the atmosphere into layers and propagating the solution through the layers, the total upwelling radiance (for a downlooking instrument) can be written in terms of four components :

$$R_{\mu} \dots = f_{\mu} R_{s, \mu} \dots + R_{\text{layer emission}, \mu} \dots + R_{\text{th}, \mu} \dots + R_{\text{solar}, \mu} \dots \quad (2)$$

which are the surface, layer emissions, downward thermal and solar terms respectively. The terms in the equation are relatively straightforward, and the resulting algorithm is usually quite efficient.

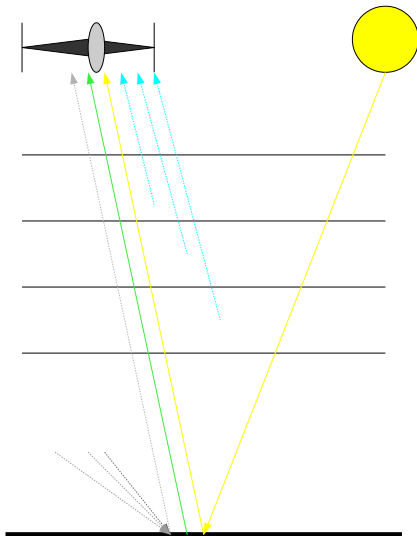


Figure 1: Illustration of contributions to measured Top Of Atmosphere radiance : (blue) layer emission, (green) surface, (yellow) solar and (gray) background thermal

Our monochromatic code kCARTA indexes the atmosphere so that layer 1 is the bottom and N ($=100$) the uppermost. Denoting $B_{\mu}; T \dots$ as the Planck function, T_s as the skin surface temperature, ϵ_s as the surface emissivity, μ as the satellite viewing angle, μ_{solar} as the sun zenith angle, $t_{j, \mu} \dots$ as the transmission of layer j ($t_{i, \mu} \dots = \exp(-k_{i, \mu} \dots)$), $t_{j \rightarrow m, \mu} \dots$ as the transmission from layer i to layer m , the individual terms are computed in monochromatic codes, such as kCARTA as follows.

2.1 Surface emission

This is simply the emission from the surface (temperature T_s), multiplied by the surface emissivity ϵ_s to account for the surface not being a perfect black body, and attenuated by absorption due to the atmosphere.

$$R_{s, \mu} \dots = f_{\mu} \epsilon_s B_{\mu}; T_s \dots + t_{s \rightarrow 1, \mu} \dots$$

2.2 Layer emission

As the radiation emitted from the surface propagates up, it is absorbed by the layer of gas above it, and then re-emitted. This atmospheric emission happens layer by layer :

$$R_{\text{layer emission}} = \sum_{i=1}^N f_i B_i(T_i) \omega_i$$

Layers with negligible absorption ($\tau_i \ll 1$) contribute negligibly to the overall radiance, while those with large optical depths ($\tau_i \gg 1$) "black" out radiation from below. $B_i(T_i)$ is the emissivity of the layer while $\omega_i = \int_0^{\pi} \int_0^{2\pi} W_i(\theta, \phi) \sin \theta d\theta d\phi$ is the weighting function W_i of the layer.

2.3 Background thermal radiation

The atmosphere also emits radiation downward in a manner analogous to the upward layer emission just discussed. Upon reaching the surface, this radiance may be reflected upward. At the surface, the magnitude of this background term is :

$$R_{\text{th}}^{\text{surface}} = \sum_{i=1}^N f_i \int_0^{\pi} \int_0^{2\pi} \tau_i(\theta, \phi) B_i(T_i) \sin \theta d\theta d\phi \quad (3)$$

Here $f_i = \int_0^{\pi} \int_0^{2\pi} W_i(\theta, \phi) \sin \theta d\theta d\phi$. Note the summation has been reversed, as we start out from the top of the atmosphere ($i = N$), and come down to ground ($i = 1$). This background thermal term also depends on the surface reflectivity ρ_s . If one assumes that the reflectivity of the surface is Lambertian, then ρ_s can be rewritten as $\frac{1}{\pi}$. This entire background reflected term is negligible in regions that are "blackened out," but in the window regions can contribute as much as 0.5 K of the total radiance when reflected back up to the top of the atmosphere.

Equation 3 involves an angular integration that needs to be done quickly but accurately. Layer by layer, the Mean Value Theorem means Eq. 3 can be rewritten in terms of an effective diusion angle θ_d^i at each layer i :

$$R_{\text{th}}^{\text{surface}} = \sum_{i=1}^N f_i \frac{1}{2} B_i(T_i) \omega_i$$

where based on the layer to ground transmissions of the i th layers, $\theta_{d1}^i, \theta_{d2}^i$ are the optimum diusion angles.

The value of θ_d^i that is often used is that of $\arccos \frac{1}{\sqrt{3}} \approx 54.7^\circ$ [1], especially for low optical depths ($\tau_i \ll 1$). A check of the accuracy of using this angle at all layers against an accurate computation using Eq. 3, showed that the errors in the window regions could be larger than 0.2 K, and would be even larger over land surfaces where the land surface emissivity is as low as 0.8. Instruments such as AIRS have channel radiance accuracies better than 0.2K, making it important to compute the background thermal correctly throughout the wavenumber region encompassed by the spectroscopic kCARTA database.

As Eq. 3 is computationally intensive, we devised the following. In an optically deep region, the surface is blacked out and one need not accurately compute the reflected term, and so $\arccos(\mu_0) \approx 0$ can be used at all layers.

Conversely in an “optically thin” region, the layers closest to the ground contribute most to R_{th} (see discussion of weighting function above). For each 25 cm⁻¹ region, the layer L above which $\arccos(\mu_0) \approx 0$ can be safely used, was determined. Below this layer, we use a lookup table where μ_0 angle is parameterized as a function of layer-to-ground optical depth (and hence transmittance).

With surface emissivity set at 0.8, L was chosen such that the brightness temperature errors at the top of the atmosphere were less than 0.1K for the sampling of profiles tested. The accuracy was checked by propagating the thermal background between the top of the atmosphere and the ground using this method, and comparing it to the results from using Eq. 3.

2.4 Solar radiation

Letting the solar reflectance be denoted by ρ_{solar} , then

$$R_{solar} = \int_{\Omega_{solar}} B_{solar} \cos \theta_{solar} d\Omega_{solar} + \rho_{solar} \int_{\Omega_{ground}} B_{ground} \cos \theta_{ground} d\Omega_{ground}$$

is usually (inaccurately) modeled as $\int_{\Omega_{solar}} B_{solar} \cos \theta_{solar} d\Omega_{solar} \approx B_{solar} \cos \theta_{solar}$. Ω_{solar} is the solid angle subtended at the earth by the sun, where r_e is the radius of the sun and d_{se} is the earth-sun distance. The solar radiation incident at the TOA B_{solar} comes from data files, and is modulated by the angle the sun makes with the vertical, $\cos \theta_{solar}$.

2.5 Monochromatic PCLSAM scattering algorithm

kCARTA can be interfaced with advanced scattering codes such as DISORT [4] and RTPSEC [5]. While well tested and numerically very accurate, these codes are complicated, leading to run times that can be significantly longer than for the clear sky case. In addition, the separation of radiative effects into solar and terrestrial means, for typical infrared instruments such as AIRS, IASI and CRiS, means one can optimize codes to work on either the thermal and/or the short wave infrared regions.

We chose to implement a fast code optimized to work where scattering is less important than absorption effects. In the thermal infrared, the effects of scattering due to aerosols and clouds is less than the effects of absorption, making the PCLSAM (Parameterization of Cloud Longwave Scattering for use in Atmospheric Models) scheme [6] very attractive. Since the model assumes the downward intensity through a cloud layer is the same as the Planck emission at the cloud temperature and thus simplifies the problem, it typically slightly overestimates the total TOA radiance. This algorithm changes the optical depth from k to a parameterized number k_0 as described briefly below; more details can be found in [6, 7].

For each layer i that contains scatterers, we replace the optical depth with the total optical depth $k_{total} = k_{atm}^{gases} + k_{extinction}^{scatterer}$. However this is reparameterized as

$$k_0 = k_{total} \left(1 - \frac{1}{b} \right) + \frac{1}{b}$$

where the effective single scattering albedo ω_0 and backscatter b_0 are obtained from the scatterer-only case ω_0 using

$$\omega_0 = \frac{f_0 \omega_0 + \dots + f_n \omega_n}{f_0 + \dots + f_n} = \frac{k_{\text{scatter}}}{k_{\text{extinction}}} \quad \dots = k_{\text{total}} \quad \dots$$

$$b_0 = \frac{f_0 b_0 + \dots + f_n b_n}{f_0 + \dots + f_n} = \frac{g_0 + \dots + g_n}{2}$$

Note that if there are no scatterers in the layer, $\omega_0 = \dots = \omega_n = 0$ and we recover the clear sky optical depth.

This same parameterization of the optical depth can be repeated for all the layers which contain scatterers, from which the radiative transfer algorithm can be written in the same form as that for clear sky radiative transfer, with very little speed penalty. Since the scattering parameters $k_{\text{extinction}}^{\text{scatterer}}$; ω_0 ; g are stored in lookup tables as a function of particle size, it is trivial to obtain the derivatives with respect to size and particle amount. This method therefore immediately lends itself to be extended to compute scattering jacobians as well as fluxes, in a manner exactly analogous to that for clear sky jacobians and fluxes.

We have attempted to account for solar scattering in the SWIR, but comparing to DISORT and actual AIRS observations, we state this a significant lien on the code in this spectral region. We note that while computing the direct beam scattered solar contribution, we use the extinction optical depth $k_{\text{extinction}} = k_0 \left(1 + e^{-k_0 \frac{1}{\sin \theta}} \right)$, rather than the parameterized optical depth k_0 .

Some points to note are that

While absorption spectra due to atmospheric gases has much structure, the crystal bonding, and smoothing over particle size distributions, "blurs" out sharp features, resulting in smooth absorption and scattering parameters.

Aerosol particles range in size from 0.1 μm (smoke) to 4 μm (dust) in diameter, which means the thermal infrared is typically much more sensitive to dust than to smoke.

Even for dust, non-sphericity of these particles is not a very big issue in the TIR. As long as realistic refractive indices are used, the results of Mie codes, integrated over realistic particle size distributions, should suffice to produce scattering parameters that can be relied upon.

Similarly water clouds can be assumed to be spherical, typically 20 μm in diameter.

Cirrus can come in many different types of shapes or "habits", which typically depend on temperature through the height of the cloud. Since the resulting ice crystals can be quite large, whose shapes can deviate significantly from spherical, Mie codes should not be used to produce scattering parameters for use in terrestrial radiative transfer codes. We use cirrus scattering parameters for ice aggregates or hexagonal plates, provided by Anthony Baran of the UKMO.

3 SARTA Clear sky Radiative transfer algorithm

Keeping the surface and layer emission terms, while ignoring the solar and background thermal terms, the monochromatic clear sky radiative transfer algorithm can be written as

of the transmittances through each layer

$$T_{\text{airs}}^{i, 1, j} \approx \prod_{l=1}^N T_{\text{airs}}^{i, l, j}$$

where $T_{\text{airs}}^{i, l, j}$ is the monochromatic transmittance through layer l .

However, this law breaks down when looking at the convolved transmittance. For example, for AIRS channel j ,

$$T_{\text{airs}}^{i, 1, j} \approx \prod_{l=1}^N \exp(-k_{i, l} \cdot \text{SR}_j \cdot \text{F}_j \cdot \text{d}_j)$$

which is NOT equal to

$$\prod_{l=1}^N \exp(-k_{i, l} \cdot \text{SR}_j \cdot \text{F}_j \cdot \text{d}_j) \neq \exp(-\sum_{l=1}^N k_{i, l} \cdot \text{SR}_j \cdot \text{F}_j \cdot \text{d}_j)$$

ie

$$T_{\text{airs}}^{i, 1, j} \approx \prod_{l=1}^N T_{\text{airs}}^{i, l, j}$$

When accounting for the convolved layer to space transmittance, not only does one have to consider the individual layers, but within each layer, the total optical depth is a sum over all contributing gases, further complicating matters. For example, for atmospheric layer i , the total monochromatic optical depth is due to a sum of contributions of all gases g such that

$$k_{i, l} \approx \sum_g k_{i, l}^g$$

from which the transmittance is $T_{\text{airs}}^{i, 1, j} \approx \prod_{l=1}^N \exp(-\sum_g k_{i, l}^g \cdot \text{SR}_j \cdot \text{F}_j \cdot \text{d}_j)$. For AIRS channel j , the polychromatic transmittance required for a Fast Model is then $T_{\text{airs}}^{i, 1, j} \approx \prod_{l=1}^N T_{\text{airs}}^{i, l, j}$, and one immediately sees a breakdown of Beer's law within the individual layers!

In the making of a Fast Forward Model, monochromatic radiative transfer becomes polychromatic radiative transfer, and the above needs to be taken into consideration. This is especially so in the case when wants to be able to consider effects of individual variable gases such as ozone, water vapor, CO2 separate from the fixed gases. SARTA handles this problem by parameterizing effective layer to space transmittances, and then converting them to equivalent optical depths for each layer. Further details are given in [8, 9].

$$T_{\text{airs}}^{\text{eff}; i, j} \approx \prod_{l=1}^N T_{\text{airs}}^{i, l, j} \approx \exp(-\sum_{l=1}^N \text{OD}_{\text{airs}}^{\text{eff}; i, j, l})$$

This means that for each layer i and AIRS channel j , we have the effective optical depth due to atmospheric gases.

4 SARTA Cloudy/aerosol sky Radiative transfer algorithm

Recall from the earlier discussion on monochromatic scattering radiative transfer, the effects of clouds and aerosols was included by simply adding in the effective scattering optical depth. For the polychromatic case, we simply add on the effects of the relevant scatterer, where needed, and then perform the radiative transfer using the clear sky algorithm. The only time penalty incurred for each cloud/aerosol contaminated column of air, is reading in and interpolating the relevant scattering tables. Since the scattering parameters vary smoothly in spectral frequency, it is very straightforward to construct scattering optical depth tables for the j th AIRS channel for scattering species S ; then for an arbitrary loading $q_{j,i} \text{ g/m}^2$

$$\begin{aligned} \text{extinction}_{j,i;r} &\propto f \text{ extinction}_{j,r} S, 1 \dots q_{j,i} S \\ \text{ssa}_{j,i;r} &\propto f \text{ ssa}_{j,r} S \\ g_{j,i;r} &\propto f g_{j,r} S \end{aligned}$$

where ssa and g are the single scattering albedo and asymmetry parameter respectively, and $\text{extinction}_{j,r} S, 1 \dots$ is the extinction for a column loading of 1 g/m^2 ; the particle size is denoted by r . The effective optical depths for channel j , layer i are then given by

$$k_{\text{airs};\text{total}}^{j,i} = f k_{\text{airs}}^{j,i} \text{gases} \dots, \text{extinction}_{\text{airs}}^{j,i} \text{scatterer} \dots$$

However again, to account for scattering effects, this is reparameterized as

$$k_{\text{airs}}^{j,i} = f k_{\text{airs}}^{j,i} f_{j,i} \text{ } 1 \dots b_{j,i} \dots g$$

where the effective single scattering albedo $f_{j,i}$ and backscatter $b_{j,i}$ are obtained from the scatterer-only case f_0 using

$$\begin{aligned} f_{j,i} \dots &= f \text{ ssa}_{j,i} \dots \text{extinction}_{j,i} = k_{\text{airs};\text{total}}^{j,i} \\ b_{j,i} \dots &= f_{j,i} \text{ } 1 \dots g_{j,i} \dots \end{aligned}$$

after which the radiance at top of the atmosphere can be calculated using the standard equations of radiative transfer.

5 Implementation details

Typically, Numerical Weather Prediction (NWP) models provide vertically resolved temperature and gas profiles at each grid point. Both k CARTA and SARTA ingest integrated versions of these profiles (via the associated `klayers` code), and use this information to compute optical depths which are then fed into the radiative transfer algorithm.

In addition, the NWP models also provide cloud fields at the same vertical resolution. When developing the SARTA-CLOUDY code, we quickly realized that although liquid water and cirrus profiles were provided, as were total cloud fractions, we would run into an infinity of problems implementing cloud fractions, and in particular overlapping cloud fractions, at each AIRS layer. For this reason, we limit the SARTA-CLOUDY code to having cloud/aerosol in at most two slabs. The input parameters for each of these slabs $k = 1; 2$ should include

species (water cloud [101], ice (habitat) cloud [201], or aerosol (type)[301])

particle effective size (in μm)

loading (in g/m^2); roughly for ice $50\text{g}/\text{m}^2 = 1 \text{ OD}$, and for water $2\text{g}/\text{m}^2 = 1 \text{ OD}$

cloud/aerosol top (mb)

cloud/aerosol bottom (mb)

cloud fraction $0 \leq c_{k,j} \leq 1$

In addition, we need a combined cloud fraction $C_{k,j}$. For channel j the total radiance at the top of the atmosphere would then be

$$R_{\text{AIRS},j} = f_{c,j} \left(c_{1,j} R_{\text{clear},j} + c_{2,j} R_{\text{cloud},j}^1 + \dots + c_{k,j} R_{\text{cloud},j}^k \right)$$

where $R_{\text{clear},j}$ is the radiance for a clear column of air, and $R_{\text{cloud},j}^k$ is the radiance assuming a column of atmosphere completely filled with cloud of type k . Obviously if $c_{1,j} = 1$ and $c_{2,j} = \dots = c_{k,j} = 0$ we get back a clear sky radiance. Depending on $c_{k,j}$ for $k \geq 1$; 2 this means at worst, the cloudy sky code is about 3 times slower than the clear sky code.

5.1 Types of scatterers

We currently have scattering tables for a number of species. The tables span the full range of 2378 AIRS channels and a range of particle sizes; hence the scattering parameters for an arbitrary effective particle size is obtained by an interpolation. In addition the tables are for a particle loading of $1 \text{ g}/\text{m}^2$; as explained above the extinction values for an arbitrary loading are obtained by a simple multiplication.

aerosol (type 301)

- desert dust
- volcanic ash
- effective diameter typically ranges from 0.5 to $10 \mu\text{m}$

cirrus (type 201)

- hex plates
- aggregates
- effective diameter typically ranges from 10 to $200 \mu\text{m}$

water (type 101)

- effective diameter typically ranges from 15 to $25 \mu\text{m}$

5.2 Cloud levels ! slabs

As mentioned above, we need to go from 90 levels of cloud profile information, to two slabs. Our "emcw2sarta" matlab routine does the necessary manipulations, summarized below.

5.2.1 Input requirements

As stated above, in addition to the usual temperature and trace gas profiles, we also need the following information from ECMWF/ERA

p.ciwc : 91xP cloud ice profiles

p.ciwv : 91xP cloud ice water profiles

p.cc : 91xP cloud total fraction

5.2.2 Smooth the input profiles

Normalize cloud profiles eg

normalized ice profile i = max(ice profile i , 0) / max(ice profile i , 0) + ...

Smooth normalized profile

normalized ice = smoothed normalized ice

5.2.3 Turn smoothed profile into slab profiles

Find how many peaks are present in this normalized profile, and "width" of peaks.

The widths will help determine the cloud top and bottom

Start combining peaks so that we have at most two peaks for ice cloud, and two peaks for water cloud

Finally, combine so at most we have two slabs

5.2.4 Determine effective particle sizes, cloud amounts and cloud fractions

Cloud amount for each slab is then determined by converting the original ice/water cloud profile (in g/g) to integrated g/m²,

Effective particle size for water is set to 20 um random amount

Effective particle size for cirrus is set according to the temperature of the cloudtop (again, a random amount).

Cloud fracs for each cloud, and the overlap, are randomly set (using the "cc" field), so that they satisfy

- c(1) = 1, c(2) = 1
- c(1,2) = min(c(1), c(2))
- clear = 1 - (c(1) + c(2) - c(1,2))
- c(1) exclusively = c(1) - c(1,2)
- c(2) exclusively = c(2) - c(1,2)

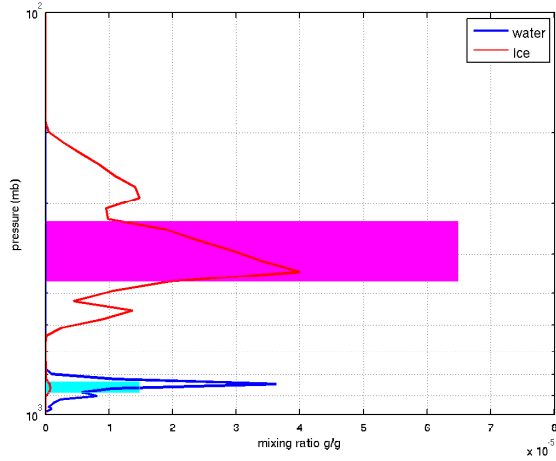


Figure 3

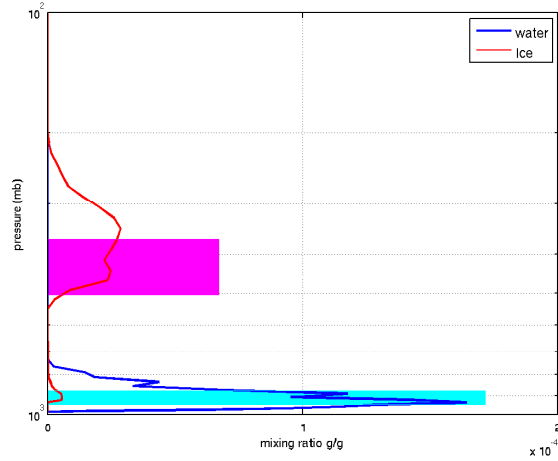


Figure 4

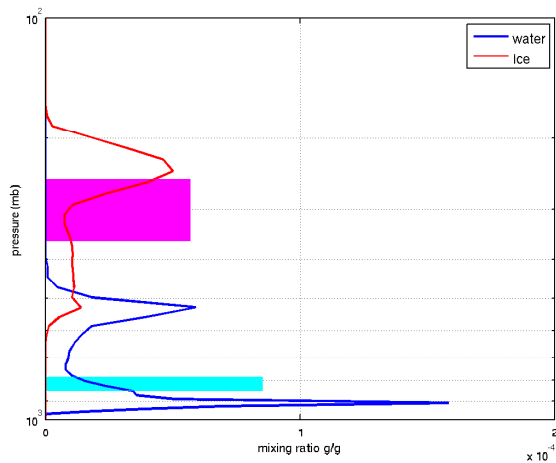


Figure 5

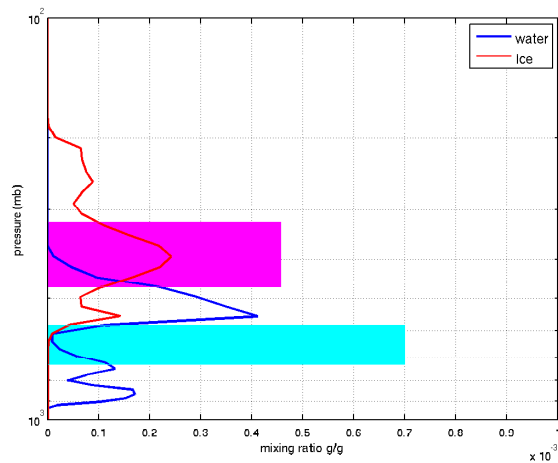


Figure 6

5.2.5 Examples

Figures 3-6 illustrate the results of our "emcwf2sarta" code. Blue and Red are the ECMWF 91 level water and ice profiles (in g/g) while cyan and magenta are the water and cirrus slabs we end up with. The horizontal extent of the slabs are the integrated cloud profiles, converted to g/m² and normalized by a factor of 10000 for the plots. It is possible to tweak the "emcwf2sarta" code in the future. For example we can move the cirrus cloud higher, if we want to reduce overall computed radiances.

6 Comparison to AIRS observations

We have been able to make some comparisons of SARTA-CLOUDY against AIRS observations, for the 10 years of data available to us. Figure 7 is a gridded map showing daytime AIRS 1231 cm⁻¹ observations (converted to BT), while Figure 8 is a similar map, showing SARTA-CLOUDY calculations, using ERA fields. Notice the overall similarities in the two figures. Obvious dif-

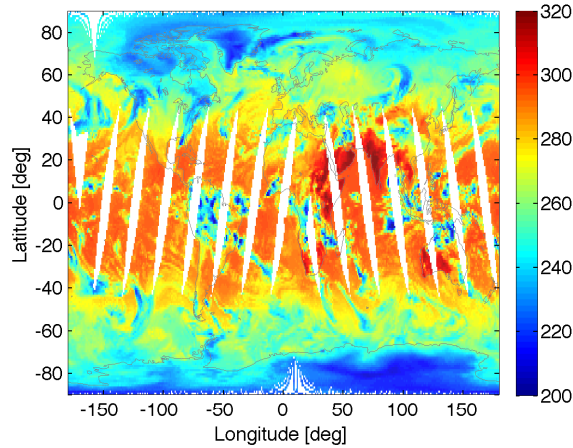


Figure 7: AIRS BT1231 cm^{-1} observations

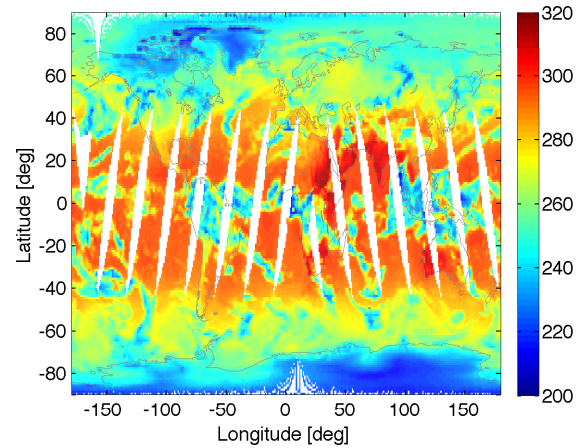


Figure 8: SARTA-CLOUDY calculations for 1231 cm^{-1} , using ERA-Interim fields

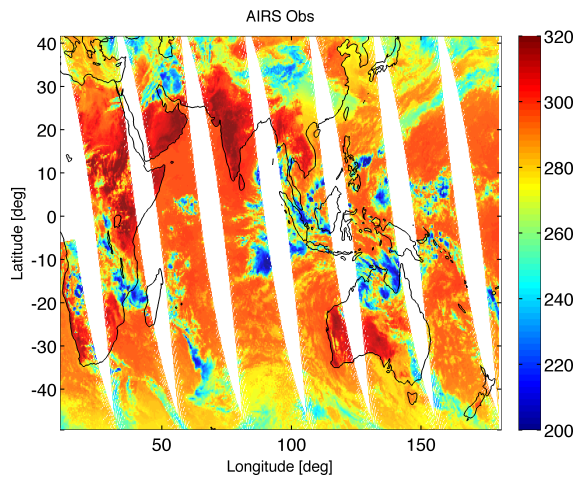


Figure 9: AIRS BT1231 cm^{-1} observations for March 11, 2011

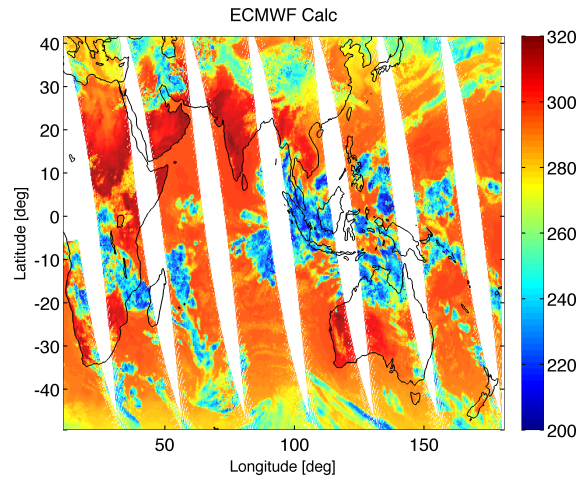


Figure 10: SARTA-CLOUDY calculations for 1231 cm^{-1} , using ECMWF fields for March 11, 2011

ferences include the DCC clouds seen in the AIRS observations, and not present in the calculations. Though not shown here, this problem is also seen when using ECMWF model fields.

The next two figures are a zoom in on the Pacific/Indian Oceans, for March 10, 2011; the SARTA-CLOUDY calculations used ECMWF fields, which are higher resolution in time and space. Figure 9 is a gridded map showing daytime AIRS 1231 cm^{-1} observations (converted to BT), while Figure 10 is a similar map, showing SARTA-CLOUDY calculations. Notice the overall similarities in the two figures.

7 Comparison to more sophisticated algorithms

We have been able to make some comparisons of SARTA-CLOUDY against PCRTM, which is a Fast Radiative Transfer code trained using DISORT. The implementation we compare against uses 50 random subcolumn incarnations of maximal overlap clouds. Other differences are that

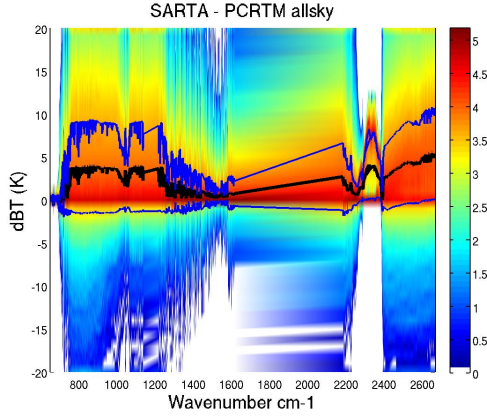


Figure 11: Comparing SARTA-CLOUDY vs PCRTM

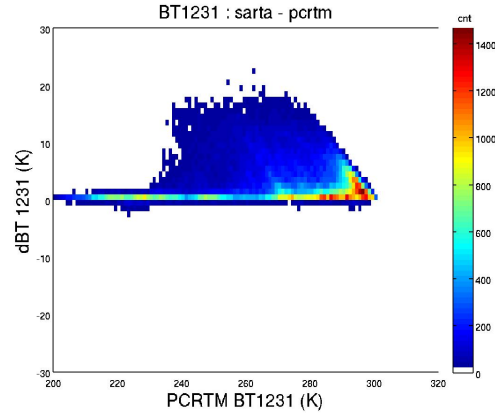


Figure 12: BT1231 comparisons

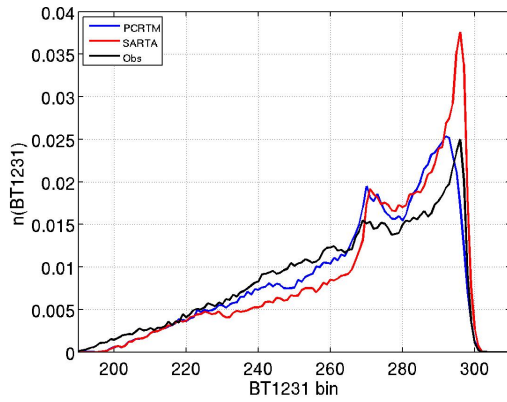


Figure 13: Comparing SARTA-CLOUDY vs PCRTM vs AIRS observations, over all the globe

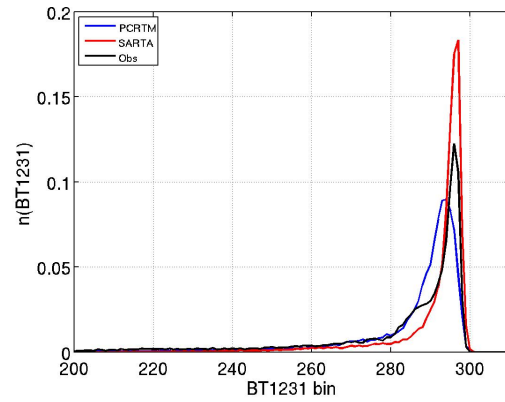


Figure 14: Comparing SARTA-CLOUDY vs PCRTM vs AIRS observations, over the Tropical Pacific

the PCRTM implementation uses ice cloud sizes that vary between 50 to 125 μm , and 20 μm water sizes, and Ping Yang's scattering parameters. The same ECMWF profiles were sent in for both SARTA-CLOUDY and PCRTM, for nadir observations for May 2012.

Figure 11 is a 2d histogram, showing bias between the two codes as a function of wavenumber. The thick black line is the mean of the bias, while the blue lines are one standard deviation away; the colorscale is the log of the number of instances. The figure shows that typically SARTA-CLOUDY produces brightness temperatures that are about 3-4 K warmer than PCRTM, for window channels. This could arise from a number of factors, such as too little cirrus cloud (either amount or fraction). To alleviate this, it is possible to tweak our "emcwf2sarta" code, as mentioned in section 4.2.5. Figure 12 shows the BT1231 cm^{-1} bias between PCRTM and SARTA-CLOUDY, as a function of computed PCRTM temperature. The colorscale is the log of the number of observations, and shows that the differences typically begin to manifest at about 260 K.

Figures 13 and 14 show the BT1231 cm^{-1} pdfs over all points on the globe, and over the Tropical Pacific. In each case, blue, red and black are the PCRTM, SARTA-CLOUDY and AIRS

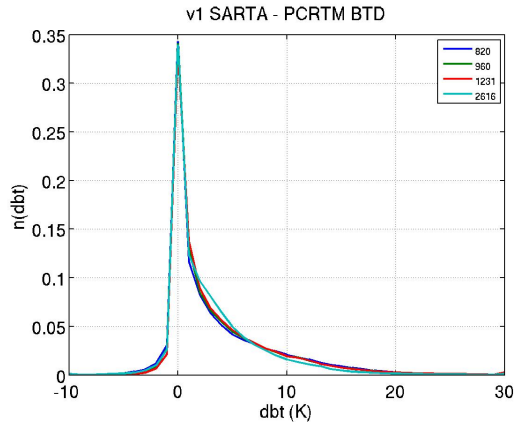


Figure 15: Comparing SARTA-CLOUDY vs PCRTM(50 subcolumns)

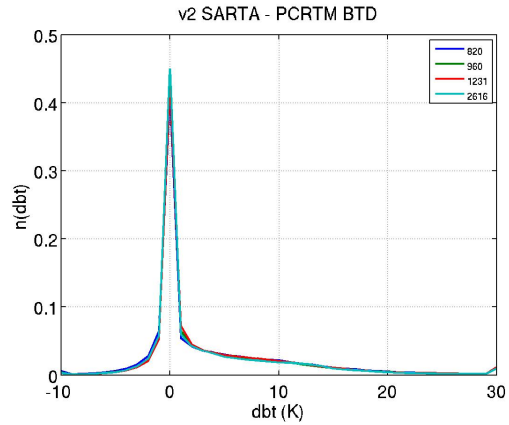


Figure 16: Comparing SARTA-CLOUDY vs PCRTM(1 subcolumn)

observations, respectively. As expected from the above discussion, typically SARTA-CLOUDY is "warmer" than PCRTM, but it is not easy to choose between the two when comparing to the AIRS observations.

While the speeds of the two codes are very similar, the architecture of our SARTA-CLOUDY is very much the same as the clear sky SARTA code, and so should be easy for a new user to learn. The user can use an ice cloud with more loading to bring the SARTA-CLOUDY line more in line with the PCRTM simulations. In addition, and perhaps more correctly, the "ecmwf2sarta" routine should be easy to modify, in order to move cirrus clouds higher up, if we feel the radiances need to be made smaller. Alternately, Figures 15 and 16 shows the night time biases between SARTA-CLOUDY and PCRTM for 820, 960, 1231 and 2616 cm^{-1} over all points on the globe. The graph on the left uses the 50 subcolumn version of PCRTM while the one on the right shows a one subcolumn version, and one sees that clearly the tail has been modified.

Importantly, even though there is a bias between the SARTA-CLOUDY and PCRTM calculations, this should not impact an operational temperature and humidity retrieval. An operational infrared AIRS L2 retrieval would need to accurately account for scattering effects when solving for temperatures and humidity. Clearly using NWP model fields which have tremendous variability, our code is producing radiances that match those from PCRTM. So it should be very possible to improve the AIRS L2 retrievals in the presence of clouds (and aerosols) using SARTA-CLOUDY. This is different from a requirement to accurately solve for cloud heights, phases, particle sizes and loadings.

References

- [1] K.N. Liou. An Introduction to Atmospheric Radiation . Academic Press, 1980.
- [2] R.M. Goody and Yung. Y.L. Atmospheric Radiation: Theoretical Basis . Oxford University Press, 1989.
- [3] D.P. Edwards. GENLN2: A general line-by-line atmospheric transmittance and radiance model. NCAR Technical Note 367+STR , National Center for Atmospheric Research, Boulder, Colo., 1992.

- [4] K. Stamnes, S.-C. Tsay, W. Wiscombe, and K. Jayaweera. Numerically stable algorithm for discrete ordinate method radiative transfer in multiple scattering and emitting layered media. *Appl. Opt* , 27:2502–2509, 1988.
- [5] M.N Deeter and F. Evans. A Hybrid Eddington Single Scattering Radiative Transfer Model for computing radiances from thermally emitting atmospheres. *JQSRT*, 60:635–648, 1998.
- [6] M.-D. Chou, K.-T. Lee, S.-C. Tsay, and Q. Fu. Parameterization for cloud longwave scattering for use in Atmospheric Models. *J. Climate* , 12:159–169, 1999.
- [7] M. Matricardi. RTIASI radiative transfer code for ECMWF, 2005. private communication.
- [8] S.E. Hannon and L. L. Strow. SARTA: The stand-alone airs radiative transfer algorithm. Technical report, University of Maryland Baltimore County, Department of Physics, <http://asl.umbc.edu/rta/sarta.html>, 2002.
- [9] L. Strow, S. Hannon, S. DeSouza-Machado, D. Tobin, and H Motteler. An overview of the AIRS radiative transfer model. *IEEE Transactions on Geosciences and Remote Sensing* , 41:303–313, 2003.